JOURNAL OF ENERGY SYSTEMS

2022, 6(4)

2602-2052 DOI: 10.30521/jes.1025810 Research Article

Development of converter configuration and corresponding control strategy for wind turbines using permanent magnet synchronous generator: A Case study

Le Van Dai

Industrial University of Ho Chi Minh City, Faculty of Electrical Engineering Technology, Ho Chi Minh City, Viet Nam, levandai@iuh.edu.vn

Submitted: 08.10.2021
Accepted: 03.10.2022
Published: 31.12.2022

Abstract: This study aims to investigate a feasible converter architecture and corresponding control method for Wind Turbine (WT) systems using permanent magnet synchronous generators (PMSG). The converter configuration is designed based on the AC/DC/AC converter, including the Diode Bridge Rectifier (DBR) and Pulse Width Modulated Current Source Inverter (PWM-CSI), Buck-Boost Converter (BBC), and Bypass Chopper (BC). The control strategy for the proposed converter is developed to enhance the operating performance of WT-PMSG, which must satisfy four requisitions. Firstly, it proposes the control approach for the pitch angle to control the output power of the WT when the wind speed is over the rated value. The selected control variables are the generator speed and active power. Secondly, the Maximum Power Point Tracking (MPPT) is archived to the satisfaction of the full-range operation through the control strategy for the BBC. The control strategy is applied by the Proportional Integral (PI) controller. The control variables are the generator speed and the diode rectifier's output DC current. Thirdly, the control strategy for PWM-CSI controls the voltage at the connection point and the frequency of the inverter. Fourthly, the DC-link voltage is controlled to the constant value at various operating conditions. Simulation of a 3MW and 0.69 kV WT-PMSG was carried on in PSCAD software to verify under considering the variable wind speed and the three-phase fault. The obtained results prove the feasibility of the proposed WT-PMSG system that serves as an alternative for a high-power wind energy conversion system.

Keywords: *AC/DC/AC converter, Electric generator, Permanent magnet synchronous generator, Wind energy conversion system, Wind turbine*

Cite this paper as: LE, V.D., Development of converter configuration and corresponding control strategy for wind turbines using permanent magnet synchronous generator: A Case study. Journal of Energy Systems 2022; 6(4): 484-502, DOI: 10.30521/jes.1025810

Nomenclature	
BtBC	Back-to-Back Converter
CSI	Current Source Inverter
DBR	Diode Bridge Rectifier
DFIG	Doubly-Fed Induction Generator
GTO	Gate Turn-Off Thyristors
MPPT	Maximum Power Point Tracking
PCC	Point of Common Coupling
PMSG	Permanent Magnet Synchronous Generator
PWM	Pulse Width Modulated
VSC	Voltage Source Converter
WECS	Wind Energy Conversion System

1. INTRODUCTION

Faced with rising energy demand, fossil energy supplies such as oil, gas, coal, and other fossil fuels are becoming more limited and creating unanticipated environmental impacts. Wind energy is one of the currently utilized potential renewable energy sources. This energy source is now one of the fastest-growing energy sources in the world. The wind energy sector achieved a new high for installation with 743 GW, a 14 % increase over the previous year. In 2020, worldwide new power installations exceeded 90 GW, an increase of 53% over 2019 [1]. Wind energy was the first source of electrical energy in the late 19th century [2].

Wind turbines (WTs) capture the kinetic energy of the wind and turn it into usable electrical energy. A dependable and efficient WT contributes to meeting the continually increasing demand for wind energy. The blades, rotor, gearbox, and generator make up a wind turbine. The WT represents more than 30% of the overall capital investment in an offshore wind project [3]. With recent advancements, a WT system may now be separated into three sections, namely dynamic, control, and monitoring [4]. Presently, the most common electric generator types in the wind-energy industry are the Doubly-Fed Induction Generator (DFIG) and Permanent Magnet Synchronous Generator (PMSG). For the DFIG, the stator is directly connected to the network, and the rotor is connected to the network via the partially-rated converter. While for the PMSG, the use of a fully-rated converter is required. Both types, in general, offer distinct advantages. However, when comparing the two, the PMSG offers various advantages, such as the ability to operate at low speeds without the use of a gearbox. Weight, size, mechanical losses, and maintenance requirements are all reduced as a result. As a result, the PMSG is becoming more prevalent in today's wind energy industry, and it is particularly well-suited to the offshore wind situation. Furthermore, the PMSG is capable of supporting the voltage at the connection point. However, losses in the power converter are a significant disadvantage of this design [5].

After integrating WT-PMSG into the existing power grid, the power system's dynamic characteristics may alter significantly. The controlling and protecting system is still a significant challenge. Even though the power electronic devices used in Wind Energy Conversion Systems (WECS) are rapidly evolving, but they are still facing technical challenges in determining WT performance in both normal and abnormal grid operations, such as maintaining optimal efficiency, withstanding grid faults, and severe weather conditions, and so on [6]. The configuration of PMSG applies to the wind energy converter through AC/DC/AC interface. Today, there are mainly three types of power electronic interface for the grid-connected WT-PMSG, namely the back-to-back converter (BtBC) using two voltage source converters (VSCs), Diode Bridge Rectifier (DBR) with VSC, and DBR with a pulse width modulated current source inverter (PWM-CSI) [7]. It depends on the use for a variety of purposes that a specific control strategy is required.

Generally, the connection methods of WT-PMSG for the variable speed wind to the network have been widely studied in recent years. The first, based on the BtBC, has been applied successfully in [8–12]. Authors in [8] have proposed the sensorless and adaptive control method. The obtained result is only tested based on low-power PMSMs. Authors in Ref. [9] have proposed the control method based on the sliding mode control to determine the control parameters. The results obtained on this method are much better than when using the conventional PI controller. Authors in [10] have investigated the event triggered-based control method for both linear and non-linear systems. Their method has very good. But this method does not consider the fractional order differential calculus. Authors in Ref. [11] have introduced the type-2 fuzzy system to improve the sliding mode control performances. Applying this method, the obtained power is maximum at all wind speeds with a maximum error 2.5 rpm of the optimum tip speed ratio. Synchronous power control has been developed in Ref. [12]. The optimization of this method is that the large-scale wind power integrates into the weak AC system. The second, based on the DBR with VSC or PWM-CSI, has been applied successfully in [7,13,14]. Authors in Ref. [7] have developed the hierarchical control for the PWM-CSI in order to improve the transient behavior. The proposed control strategy used the adaptive PI controller that is self-tuned based on a linear

approximation of the system. As a result, the proposed system has high efficiency and reliability. Authors in Ref. [13] used the indirect vector control method to control the maximum power. When applying this converter configuration and corresponding control strategy, the obtained power is maximum from the wind turbine at different wind speeds. A topology of the PWM with a multilevel current source inverter (CSI) for the grid side converter has been developed by authors in Ref. [14]. This topology is an attractive solution for large direct-drive WECSs can reach megawatts.

From a technical point of view, the BtBC with the complexity control methods allows the WT-PMSG to have excellent operating performance at a high cost. In addition, this configuration raises some technical concerns as reduced fidelity due to the high component count, low efficiency, and increased cost [15]. The DBR and PWM-CSI with simple control, on the other hand, are less costly and more dependable. As known, the power flow for the WT-PMSG is usually unidirectional from the generator to the grid. Therefore, the DBR can be applied to the generator side converter to save cost and simplify the control approach [16]. So, this configuration with a control strategy for the WT-PMSG is proposed to study in this paper. The converter configuration is developed as the AC/DC/AC power converter consisting of a DBR, a Buck-Boost Converter (BBC), a boost DC/DC converter, and a three-phase inverter. The generator side converter is designed using the DRB and BBC, with the control strategy that allows for extracting the maximum power from the wind. The grid side converter is developed using the PWM-CSI with the AC voltage control scheme. In addition, the control strategy of the blade pitch angle is also proposed to capture the optimal power from the variable wind speed. The contribution and innovation of this study may be summarized as follows:

(i) The WECS configuration cooperating with the PWM-CSI, BBC, and DBR is proposed for high-power WECS using PMSG.

(ii) The developed control strategy can provide a simple and reliable solution for generator power rectification and improve the grid connection capacity of the WECS.

The rest of the paper is organized as follows: The goal of Section 2 is to create a PMSG-WESC arrangement for converting wind energy to electrical energy. Meanwhile, Section 3 proposes the corresponding control technique. Section 4 verifies, analyzes, and discusses the effectiveness of the suggested configuration and control. Finally, in Section 5, the conclusions are summarized.

2. WIND ENERGY CONVERSION SYSTEM CONFIGURATION

This section aims to provide the model of PMSG-WESC for converting wind energy to electrical energy. The structure of PMSG-WESC is considered for this study, as shown in Fig. 1, consisting of the main parts as the wind turbine, synchronous generator, and converter stage AC/DC/AC, controller units, and other parts. The details of these parts will be described in the following sub-section.

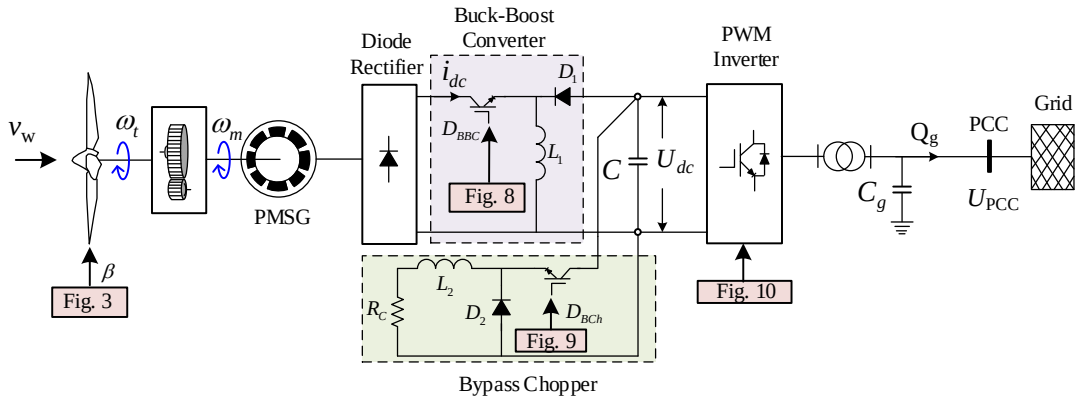

Figure 1. The proposed configuration and control of PMSG based on WECS.

2.1. Wind Turbine

Fig. 2 describes the wind turbine under aerodynamic mode. The wind turbine is the device used to convert the linear motion of the wind into mechanical rotational motion. The output mechanical power P_m and torque T_m can be respectively derived as follows [17,18]:

$$P_m = \frac{1}{2}\rho\pi R_t^2 C_p(\lambda,\beta)v_w^3 \tag{1}$$

$$T_m = \frac{1}{2}\rho\pi R_t^3 \frac{C_p(\lambda,\beta)}{\lambda^3}v_w^2 \tag{2}$$

where v_w is the wind speed, R_t is the length of the blade of the wind turbine, ρ is the air density, and C_p is the power performance coefficient. Observing Eq. (1), if the wind speed, air density, and swept area are supposed to be constant, the aerodynamic power depends on C_p. In this paper, This C_p is calculated based on the information of blade geometry and element theory and can be approximately described as follows [19] :

$$C_p(\lambda,\beta) = 0.5176\left(116\left(\frac{1}{\lambda+0.08\beta}-\frac{0.035}{\beta^3+1}\right)-0.4\beta-5\right)e^{-21\left(\frac{1}{\lambda+0.08\beta}-\frac{0.035}{\beta^3+1}\right)} + 0.006795\left(\frac{1}{\lambda+0.08\beta}-\frac{0.035}{\beta^3+1}\right) \tag{3}$$

in which β is the pitch angle, λ is the tip speed ratio, and determines as follows:

$$\lambda = \frac{\omega_m R_t}{v_w} \tag{4}$$

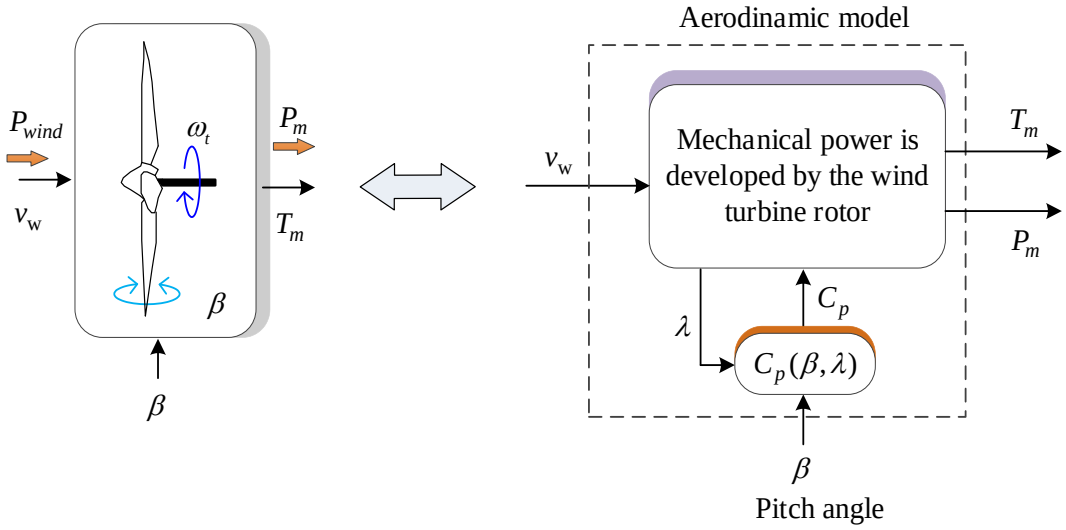

Figure 2. The block diagram of the aerodynamic model of a wind turbine.

2.2. Synchronous Generator

In this study, the control system for the PMSG-WECS is developed base on the *dq* synchronously rotating reference frame. The following equations establish the dynamic model of SG. The stator voltage equations are as follows [20,21]:

$$u_{ds} = -R_s i_{ds} + \omega_e L_q i_{qs} - L_d \frac{d}{dt} i_{ds} \quad (5)$$

$$u_{qs} = -R_s i_{qs} - \omega_e L_d i_{ds} + \omega_e \lambda_r - L_q \frac{d}{dt} i_{qs} \quad (6)$$

where R_s is the resistance of the stator; λ_r *is* the flux linkage of the rotor; i_{ds} and i_{ds} are the *d*-axis and *q*-axis currents, respectively; u_{ds} and u_{dr} *are* the *d*-axis and *q*-axis voltages, respectively; L_d and L_q *are* the *d*-axis and *q*-axis synchronous inductances, respectively. The electromagnetic torque equation is as follows [22]:

$$T_e = 1.5 z_p \left(\lambda_r i_{qs} - (L_d - L_q) i_{ds} i_{qs} \right) \quad (7)$$

The ω_e is the electrical angular velocity and ω_m is the mechanical speeds which are respectively obtained as follows:

$$\omega_e = \frac{z_p}{J} \int (T_e - T_m) dt \quad (8)$$

$$\omega_m = \frac{\omega_e}{z_p} \quad (9)$$

where J is the moment of the inertia, T_m is the mechanical torque obtained from Eq. (2), and z_p is the number of pole pairs.

3. PROPOSED CONTROL STRATEGY

The proposed system is shown in Fig. 1, including the turbine and the AC/DC/AC converter and the pitch controller. Their control strategy is featured in the following subsections.

3.1. Pitch Controller

The control strategy of the blade pitch angle, as shown in Fig. 3, is used in this study. For this proposed strategy, the output power of WT depends on wind conditions. Thus, the blade pitch angle regulation can be spilt the excess power when the wind speed overshoots the nominal. The reference speed and actual power are two signals chosen to compare their real values. The error signal of speed and the active power has derived the gains (K_s and G_m) and PI controller, respectively. These output signals are compared and actuated to generate the β signal, where the actuator proposed a lag between the inverse error signal (β*) from the PI controller and (K_s and G_m) and the actual β signal. Therefore, the obtained output power based on Eq. (1) depends on the wind speeds. The output power is equal to zero when the wind speeds are less than the cut-in speed threshold or exceed the cut-out speed threshold. This means that the turbine does not turn or is stopped. The output power is less than the rated one, and the obtained power depends on the wind speed that corresponds to β equal to zero. The output power is equal to the rated one that corresponds to β not zero. All assumptions can be shown in Fig. 4.

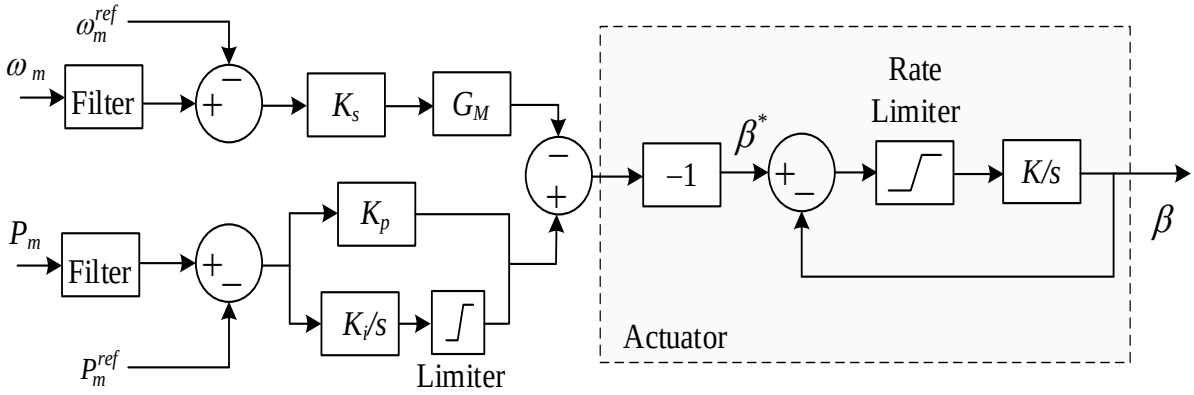

Figure 3. The proposed pitch angle controller.

The captured power is dependent on the wind speed. For the wind speed between zero and the cut-in speed, the captured power is insufficient to forereach the rotor inertia and friction. This leads to the wind turbine in a standstill condition. For the wind speed between the cut-in and rated speed, the power can be captured from wind speed using MPPT. The wind energy is fully exploited for the speed between rated speed and cut-out speed, and the wind turbine is controlled to capture the rated power. For the speed that is greater than the cut-out speed, the captured power is too big, and the turbine is operated under the forced condition to stop to prevent it from damage.

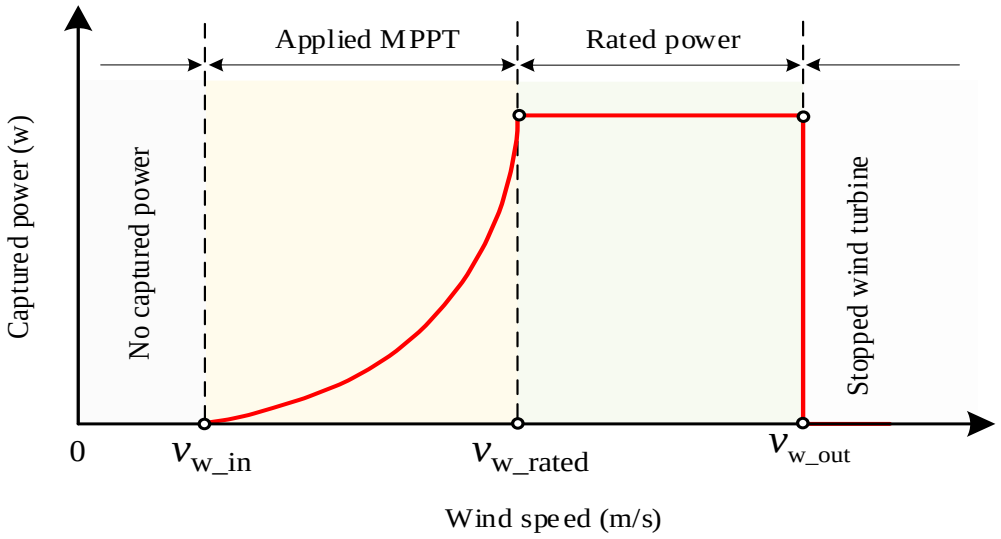

Figure 4. The output power characteristic under different wind speeds of WECS.

When the WT operates at a zone that the wind speed is from v_{w_in} to v_{w_rated}, the pitch angle control is active. The MPPT is applied, and the turbine speed is controlled so that the C_p would achieve a maximum value. The generator rotor mechanical speed reference at the maintained maximum active power can be calculated based on the corresponding optimum tip speed ratio as follows:

$$\omega_{m\_opt} = \frac{\lambda_{opt} v_w}{R_t} \tag{10}$$

Observing Eqs. (1) and (10), it can be concluded that when MPPT worked, the WT-PMSG was operating under optimal conditions. As a result, the rotational speed and the mechanical power are proportional to the first-order and cubic rate of wind speed according to the aerodynamic characteristic of the wind turbine, respectively.

3.2. AC/DC/AC Conversion

The wind speed is the variable, and it leads to the variable of the output voltage and frequency of PMSG. Therefore, the AC/DC/AC conversion must be applied to create the constant frequency and voltage when PMSG is connected to the network. The AC/DC/AC converter is an architecture that uses a diode rectifier for the generator side and PWM-CSI for the grid side to balance performance and cost.

3.2.1. Buck-boost Converter

A simplified model in the *dq* reference frame is shown in Fig. 5, which is derived based on Eqs. (5) and (6). This model is valid for both non-salient- and salient-pole PMSG [20]. For the non-salient type, the *dq*-axis synchronous inductances are equal, whereas they are different for the salient one. Noting that, the *d*-axis synchronous inductance of PMSG is usually lower than that of the *q*-axis one [23].

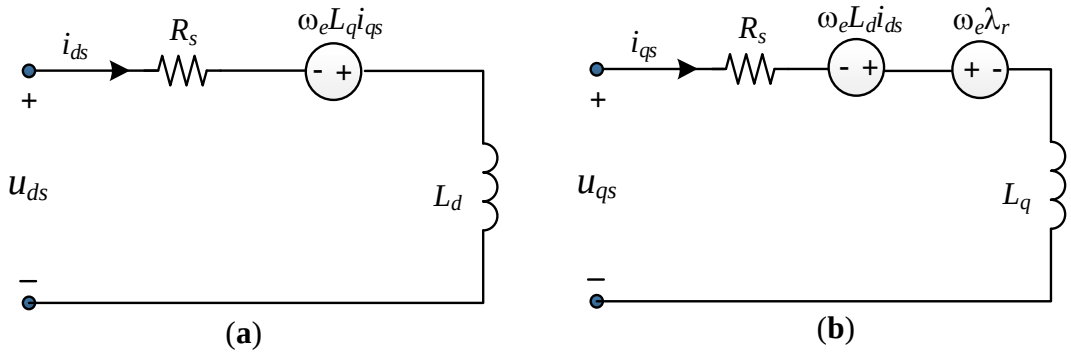

*Figure 5. The dq-axis model of the PMSG in the rotor-field synchronous reference frame: (**a**) d-axis circuit; (**b**) q-axis circuit*

The multi-pole PMSG type is chosen in this study to be non-salient; the *d- and q*-axis synchronous inductances are approximately equal. Therefore, the *dq*-axis model of PMSG can be simplified as the equivalent phase circuit as shown in Fig. 6(a), and the phasor diagram is described in Fig. 6(b), in which X_s and R_s are the synchronous reactance and resistance of the per phase stator winding, respectively. I_s and U_s are the stator current and voltage in the per phase, and E_s is the induced electromotive force in the per phase stator winding and can be expressed as follows [24]:

$$E_s = \omega_e \lambda_r \tag{11}$$

where λ_r is the rotor flux and ω_e is the electrical angular velocity. The corresponding vector equation can be obtained by basing on Fig. 6 (a) as follows:

$$\dot{E}_s = \dot{U}_s + \dot{I}_s R_s + jX_s \dot{I}_s \tag{12}$$

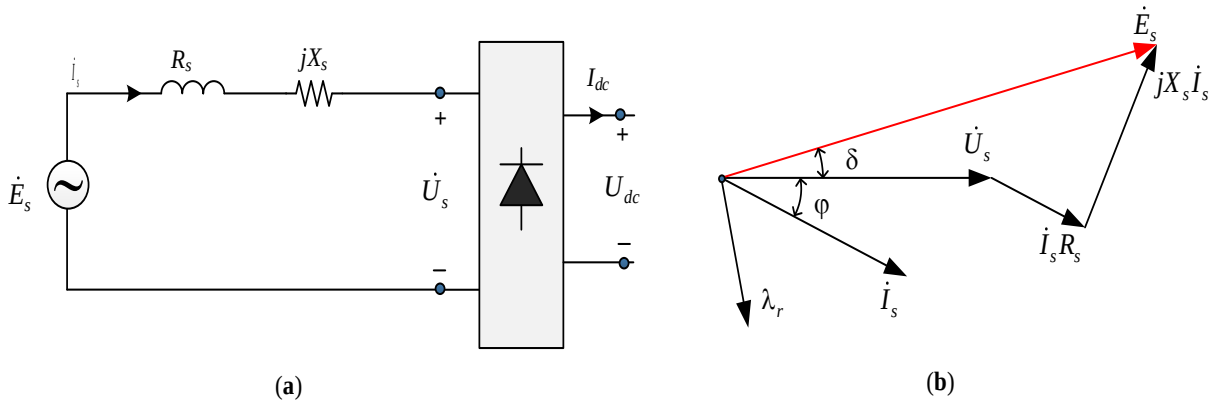

(**a**) (**b**)

Figure 6. The equivalent circuit of PMSG: (a) equivalent per phase circuit, (b) phasor diagram.

The output diode rectifier voltage is obtained under the condition of the commutation angle δ (0 < δ < 60°) as follows [25]:

$$U_{dc} = \frac{3\sqrt{2}}{\pi} E_s - \frac{3}{\pi} X_s I_{dc} \tag{13}$$

The commutation angle δ as shown in Fig. 6(b) can be calculated as follows:

$$\cos\delta = 1 - \frac{\sqrt{2} X_s I_{dc}}{E_s}, (0 < \delta < 60^o) \tag{14}$$

Assuming that the loss is neglected, the obtained power from the wind is transferred to the DC side is:

$$P_{dc} = U_{dc} I_{dc} = P_s \tag{15}$$

Substituting Eq. (13) into Eq. (15) gives,

$$P_{dc} = U_{dc} I_{dc} = (\frac{3\sqrt{2}}{\pi} E_s - \frac{3}{\pi} X_s I_{dc}) I_{dc} = P_s \tag{16}$$

The current of the diode rectifier can be calculated as follows:

$$I_{dc} = \frac{3\sqrt{2} E_s \pm \sqrt{18E_s^2 - 12\pi\omega_e L_s P_s}}{6\omega_e L_s} \tag{17}$$

It can be derived from Eq. (17) that a constrain of the system parameters should be satisfied to ensure the real solution of I_{dc}, as illustrated in Eq. (18). When this condition is satisfied, the I_{dc} is a real solution, which means the MPPT can be achieved. From Eq. (17), I_{dc} can be calculated through the parameters of the generator and wind turbine

$$E_s \geq \sqrt{\frac{2}{3}\pi\omega_e L_s P_s} \tag{18}$$

Based on Eqs. (1) and (10), and the condition in Eq. (18) is satisfied, the two solution values of I_{dc} in Eq. (17) are positive. However, only the smaller solution value satisfies the pre-conditions as given in Eq. (14). This means that for certain PMSG parameters and specific wind turbine speeds, the DC current

is definite at the output of DRB. As a result, Fig. 7 shows the relationship between the wind speed and the DC current with the difference between rotor flux and stator inductance value for the proposed configuration.

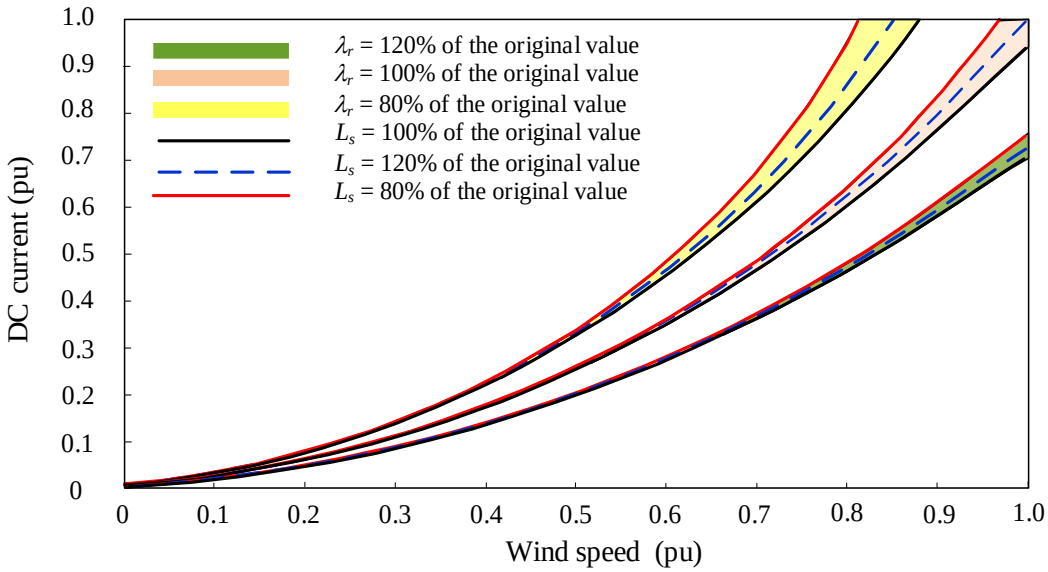

Figure 7. DC link current produced by diode rectifier based on system parameters

Fig. 8 shows the control diagram for the BBC to be the satisfaction with the full-range operation of MPPT. This control strategy consists of two loops using the PI controller in which the slower outer loop is applied for the speed control, and the fast inner loop is applied for the out DC current control of the diode rectifier. If the DC current reaches the value of 1 pu under the rated wind speed value of 1 pu, the λ and L_s can be definite, and this condition is considered as original values.

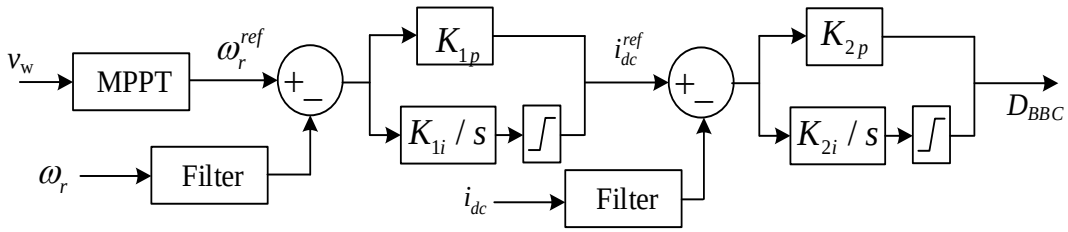

Figure 8. Buck-Boost converter controller.

3.2.2. Bypass chopper

As known, when the sag voltages occur, the generator's output power may exceed the maximum level. So that the voltage on the DC-link increases. To solve the problem, this study proposes the boost DC/DC converter with a control strategy, as shown in Fig. 9 [26].

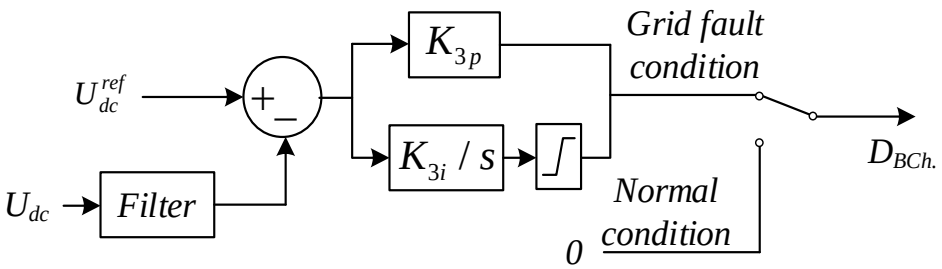

Figure 9. Bypass chopper controller.

3.2.3. Grid side converter control

Two conditions must be attentive at the integration point between the network and wind turbine. The first condition is the voltage at the connection point must be 1pu, and the voltage control needs to be done at the connection point instead of at the DC link. The second condition is the frequency of the inverter must be contained on grid frequency. Therefore, it must use the phase lock loop. The control scheme in this study is AC voltage control [27]. This control is realized based on the pulse with modulation (PWM), as shown in Fig. 10, and the drive of this device can be divided into three parts that are the generation of the triangular waveform, the reference, and the firing pulses of the 6 GTO of the inverter.

The generation of the triangular waveform: this part is shown in the yellowish part of Fig. 10(a). The instantaneous measured voltage is split into three-phase components that are given as input signals to a three-phase PI-controlled PLL. It generates a ramp signal at the system frequency and is then increased by a real constant $K_{trg.}$ In this study, $K_{trg.}$ is equal to 33. In order to generate the ramp signal to the triangular signal, the angle resolver is applied to retrain the ramp signal to between zero and 360 degrees at the carrier frequency. The code for realizing the angle resolver is listed in Table 1. The non-linear transfer function is used to transform the triangular signal to the carrier frequency at each period with amplitude from -1 to 1. This triangular signal can be divided into two compensatory arrays ones called Trg._On and Trg._Off.

The generation of the reference: this part is shown in the pink part of Fig. 10(a). The instantaneous measured voltage is split into its three-phase components that are given as input signals to a three-phase PI-controlled six-pulse PLL. The input ramp array signals from six generated signals synchronized on the measured output voltage of the inverter are shifted by an error signal between the $K_{ref.Sign.}$ and control voltage loop signal "Angle order". In this study, $K_{ref.Sign.}$ is equal to 30 and the "Angle order" signal is obtained from the control voltage loop as shown in Fig. 10(b). The code for realizing "Shift" is listed in Table 1. The out signals are sent to the sinusoidal function block to converter the required sinusoidal waveforms. These signals are divided into two complementary arrays of sinusoidal waveforms called Ref.Sign._On and Ref.Sign._Off.

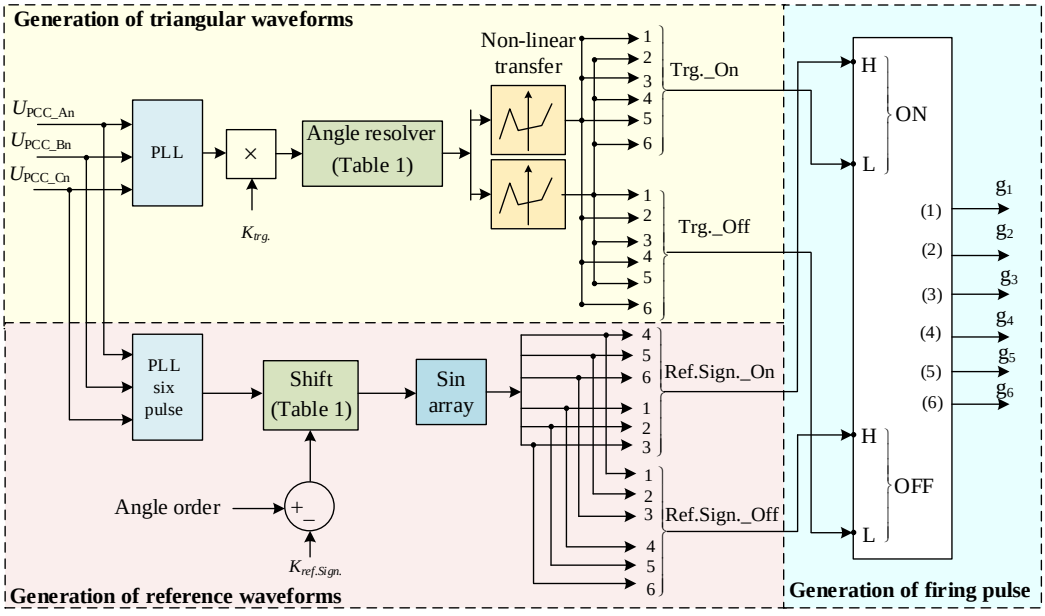

(a)

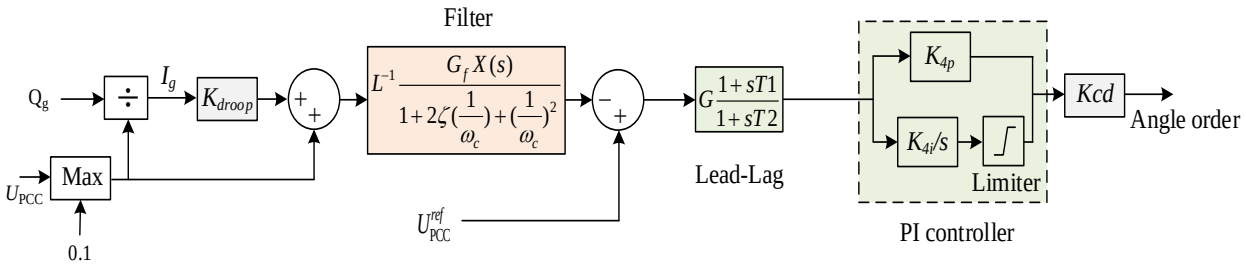

(b)

Figure 10. The grid converter control strategy: (a) The pulse with modulation regulation drive, (b) the voltage control loop.

Table 1 Method to generate triangular and reference waveforms.

Method 1: Angle Resolver

```
$phiout = ATAN2(SIN($phiin~
#CASE IPUnit {~~} {~*PI_BY180~}
~),COS($phiin~
#CASE IPUnit {~))~} {~*PI_BY180))~}
#CASE OPUnit {~} {~*BY180_PI}
#IF OPRange==1
      IF ($phiout .LE. 0.0) THEN
        $phiout = $phiout + ~
 #CASE OPUnit {~TWO_PI} {~360.0}
      ENDIF
#ENDIF
```

Method 2: Shift

```
 DO i=1,6
   $out(i)=$in(i)-$phsh
   IF ($out(i).GT.360) $out(i)=$out(i)-360.0
   IF ($out(i).LT.0.0) $out(i)=$out(i)+360.0
ENDDO
```

The generation of the firing pulses of the 6 GTO of the inverter: this part is shown in the pale blue part of Fig. 10(a). In this study, the interpolated firing pulse, introducing in PSCAD, was proposed to use. The inputs are the reference signals and the triangular waveforms. The output signals are the firing pulses of g_1, g_2,..., and g_6 that are produced by comparing input signals between high (*H*) and low (*L*) levels. These firing pulses use to open and close switches of thyristor GTO. Fig. 11 shows the generation of the g_1 GTO pulse.

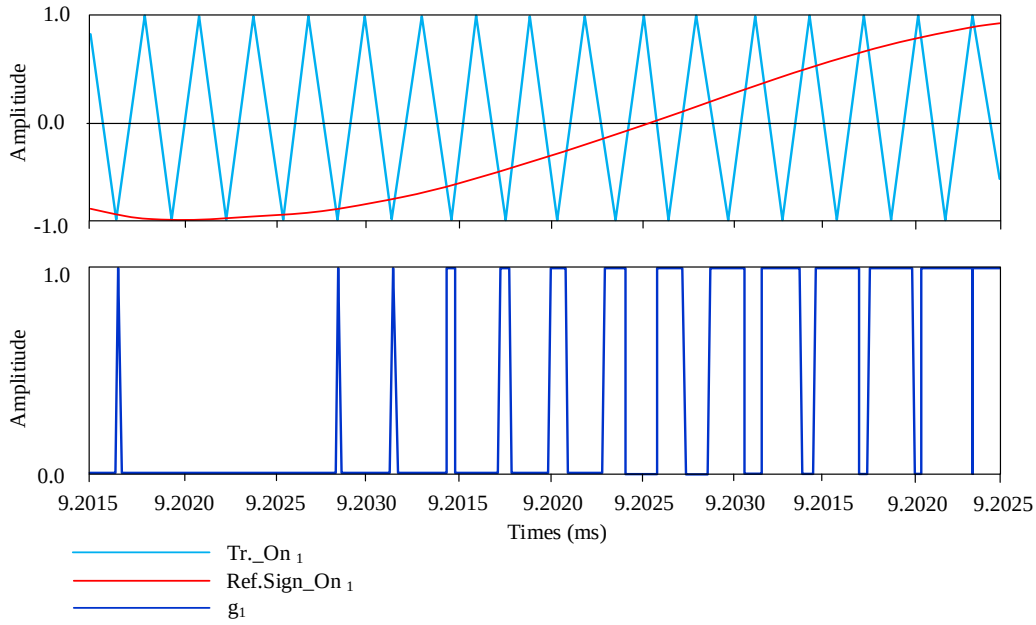

Figure 11. The input and output signal for generating the g_1 GTO pulse.

4. SIMULATION AND ANALYSIS

The three-bus 12.47 kV network, as shown in Fig. 12, is proposed for the use of simulation in this study**.** This network includes three loads provided by the 300 MVA source through a Y/Y transformer with a ratio of 34.5 kV: 12.47 kV. The 3MW-0.69 kV WT-PMSG is connected to the network 12.7 kV at Bus 2 through Y/Y transformers. The ratio of the cage and main transformers are 0.69 kV:12.47 kV. The wind speed under normal conditions is 12 m/s. All concerned parameters are listed in Table 2.

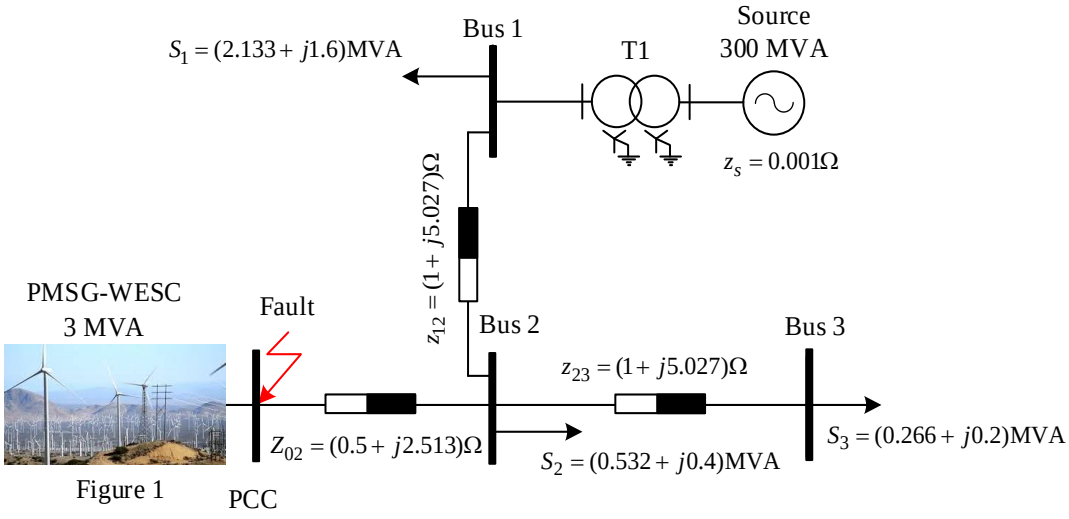

Figure 12. The proposed power system for simulation.

4.1. Case 1: Variable Wind Speed

This case will illustrate the convenience of MPPT to the proposed configuration and control scheme under undergoing a change of the wind speed concerning the time, as shown in Fig. 13. The simulation results of the mechanical and electrical variables are shown in Figs. 14 and 15, respectively.

Table 2. The parameters for the proposed WT-PMSG.

	Parameter	Value
3.6 MW horizontal axis WT	Number of blades	3
	Cut in speed	4 m/s
	Cut out speed	25 m/s
	Rated speed	12 m/s
	Air density	1.225 kg/m^2
	Blade radius	46.2 m
3 MVA-PMSG	Rated power	3 MVA
	Rated voltage	0.69 kV
	Rated rotor speed	22 rpm
	Rated rotor flux linkage	32.6 mWb
	Stator winding resistance	0.0168 Ω
	Number of pole pairs	100
DC-link	DC capacitor	2100 μF
	DC inductor	48.8 mH
Bypass Chopper	DC capacitor	1900 μF
	DC inductor	67.6 mH
	K_{3p}	2.45
	K_{3i}	0.75
Buck-Boot converter	K_{1p}	3.25
	K_{1i}	0.45
	K_{2p}	5.35
	K_{2i}	0.6
Voltage control loop	K_{droop}	0.03
	T_1	0.007 sec
	T_2	0.0001 sec
	K_{cd}	40
	K_{4p}	1.4
	K_{4i}	0.4
	G	1.0
	G_f	1.0
	ξ	0.7
	$\omega_c=2\pi f_c$	75Hz

Observing Fig. 14, if the wind speed is lower than 12 m/s, the pitch angle equals zero, the generator speed will be regulated to reach MPPT, and the tip-speed ratio does not change. When wind speed exceeded the rated speed of 12 m/s, the pitch angle was activated and changed from zero to 4.5 degrees. The power coefficient was regulated from 0.467 to 0.417. The BBC is active in satisfying the full-range operation of MPPT and the balance between the generation of power and the requirement of the load. The oscillations of mechanical variables in this case as the pitch angle, the generator speed, the power coefficient, the tip-speed ratio, and the active power are shown in Figs. 14 (a–e), respectively.

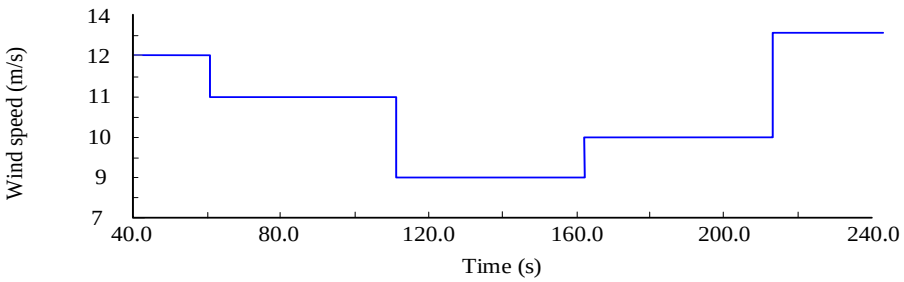

Figure 13. The proposed power system for simulation.

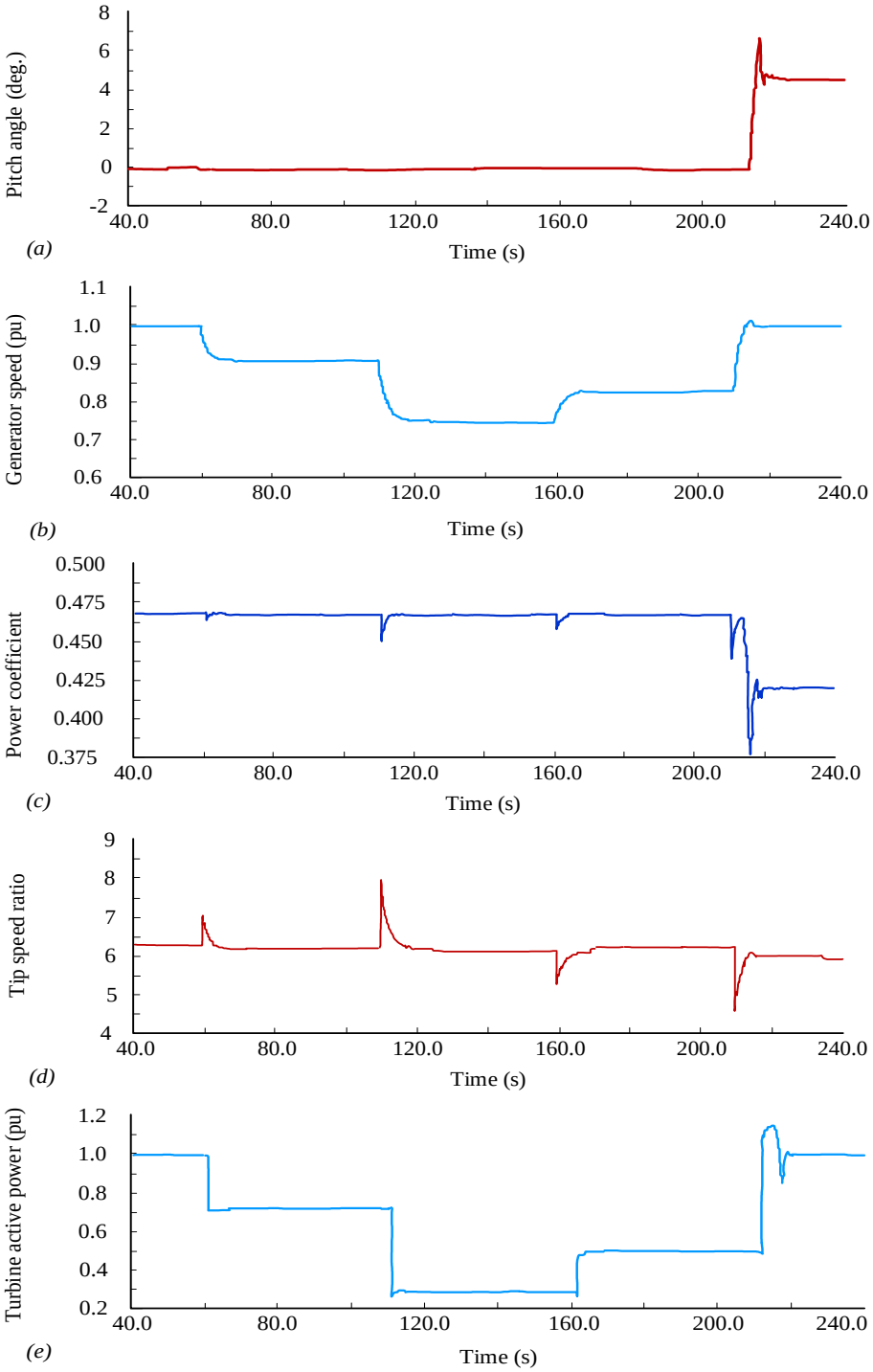

Figure 14. Simulation results of mechanical variables under the wind profile in Figure 13: (a) Generator speed, (b) tip speed ratio, (c) pitch angle, (d) power coefficient, (e) turbine active power.

Concerning the electrical variable simulation results as shown in Fig. 15, the oscillations of DC-link voltage is in the range ± 0.4 % as shown in Fig. 15(a), it was guaranteed at a level sufficient to satisfy the DC to AC conversion requirements, which indicates that the generated active power due to the wind turbine is glidingly transmitted to the network at Bus 2 as shown in Fig. 15(b). The oscillations of voltage at the point of common coupling (PCC) occur because of causing the change of reactive power consumption in the transformer and on transmission lines. This problem can be seen in Fig. 15(c) corresponding to the voltage at PCC and in Fig. 15(d) corresponding to the reactive power. The voltage at PCC with unity power factor dropped by 1.5 % because of the change of reactive power from 0 to 0.1 pu. In addition, the voltage at PCC fluctuated with turbine speed but not significantly. Thus, it can be

concluded that the proposed control strategy as shown in Fig. 10(a) can reduce the oscillations of voltage at PCC when the wind speed changes.

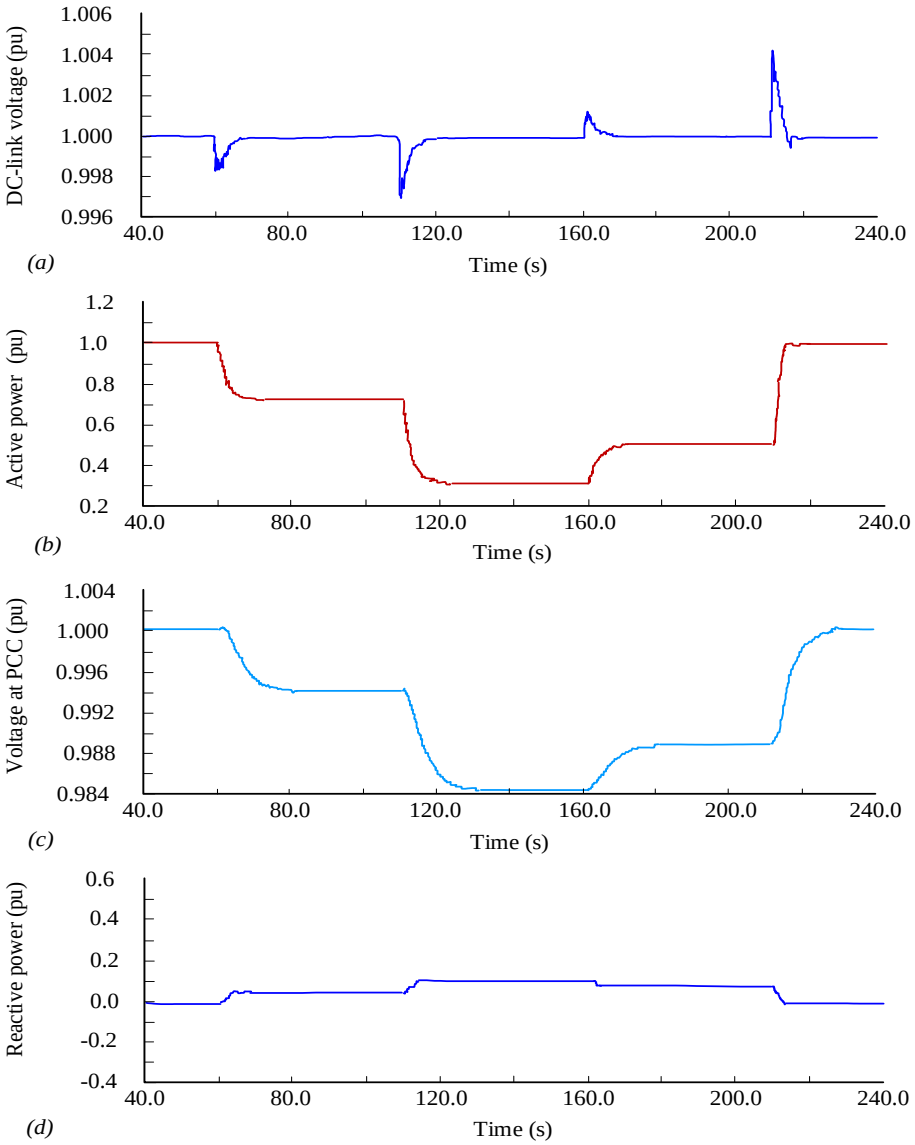

Figure 15. Simulation results of electric variables under the wind profile as shown in Figure 13: (a) DC-link voltage, (b) active power, (c) voltage at PCC, (d) reactive power.

4.2. Case 2: Grid Fault

The transient response of the proposed PMSG's configuration is tested by considering a three-phase to ground fault at PCC, as shown in Fig. 12. The wind turbine is operating at the rated wind speed of 12 m/s during the simulation. A three-phase to the ground is considered in this case because of its severity. Based on the requirement of grid-connected code in [28]. The AC voltage at PPC is shown in Fig. 16 when the three-phase to ground fault occurred at PCC, starting and clearing at 80.6s and 80.74s, respectively, with zero voltage dip with a clearance time of 0.14s. The wind turbine is operating at the rated wind speed of 12 m/s. The simulation results of the system response under the mechanical and electrical variables are shown in Figs. 17 and 18, respectively.

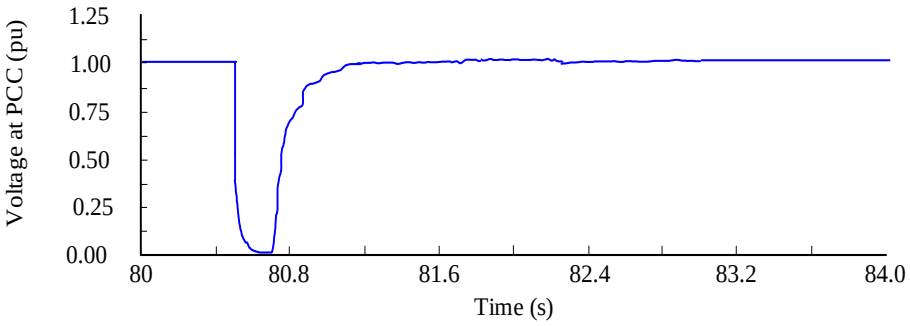

Figure 16. The voltage profile at PCC.

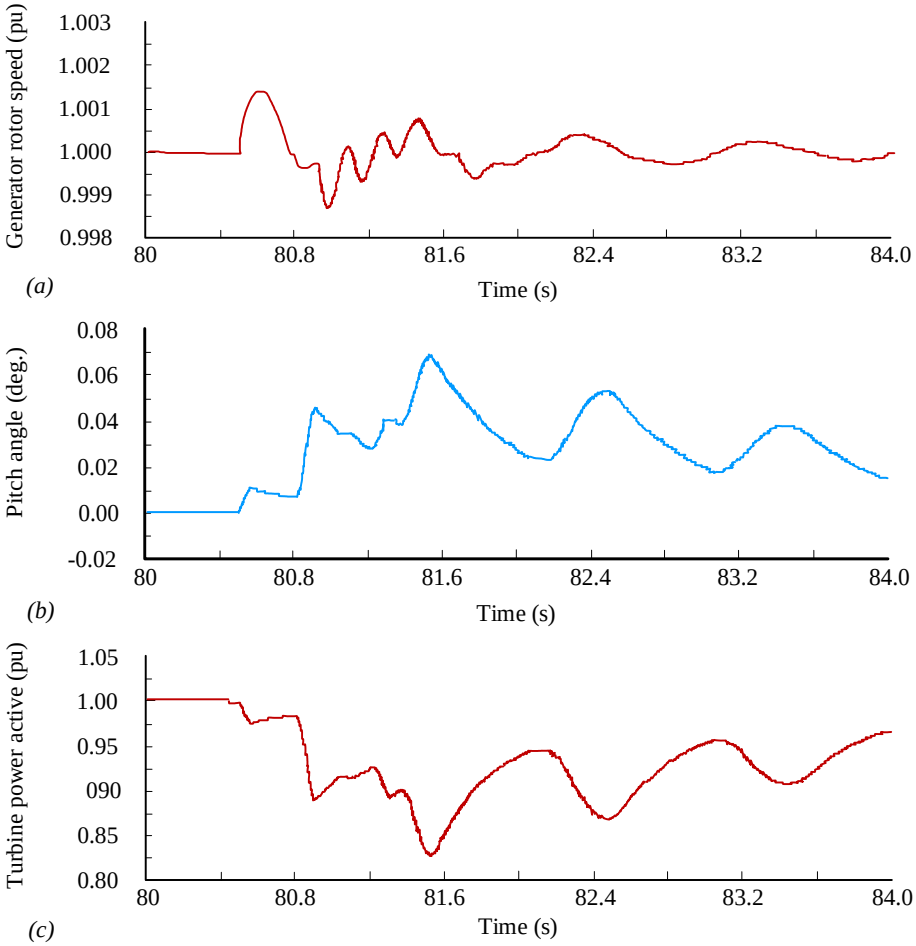

Figure 17. Simulation results of mechanical variables under fault state: (a) Generator speed, (b) pitch angle, (c) turbine active power.

The fault occurred, and the generator speed temporarily increased, as shown in Fig. 17(a). The pitch sparked off to keep the system stable, as demonstrated in Fig. 17(b). Another mechanical variable, being the active power of the turbine, has violently oscillated, as shown in Fig. 17(c). Fig. 18(a) shows the DC-link voltage. This voltage has instantaneously oscillated, and this oscillation will be damped when the fault is cleared. The bypass chopper is sparked off during a fault to hold the voltage around the capacitor at the normal value. Due to the imbalance of power flow between the grid and DC-link, the active power is not transferred into the grid that can be absorbed from the grid, as shown in Fig. 18(b). The reactive power is controlled. Therefore, it is normally equal to zero. This reactive power is instantaneously increased when the grid voltage dip, as shown in Fig. 18(c). After clearing the fault, all

electrical and mechanical variables are restored quickly. The system quickly returns to steady-state, and specifically, the reactive and active powers, the voltage at PCC, and DC-link are restored after 1.6 sec.

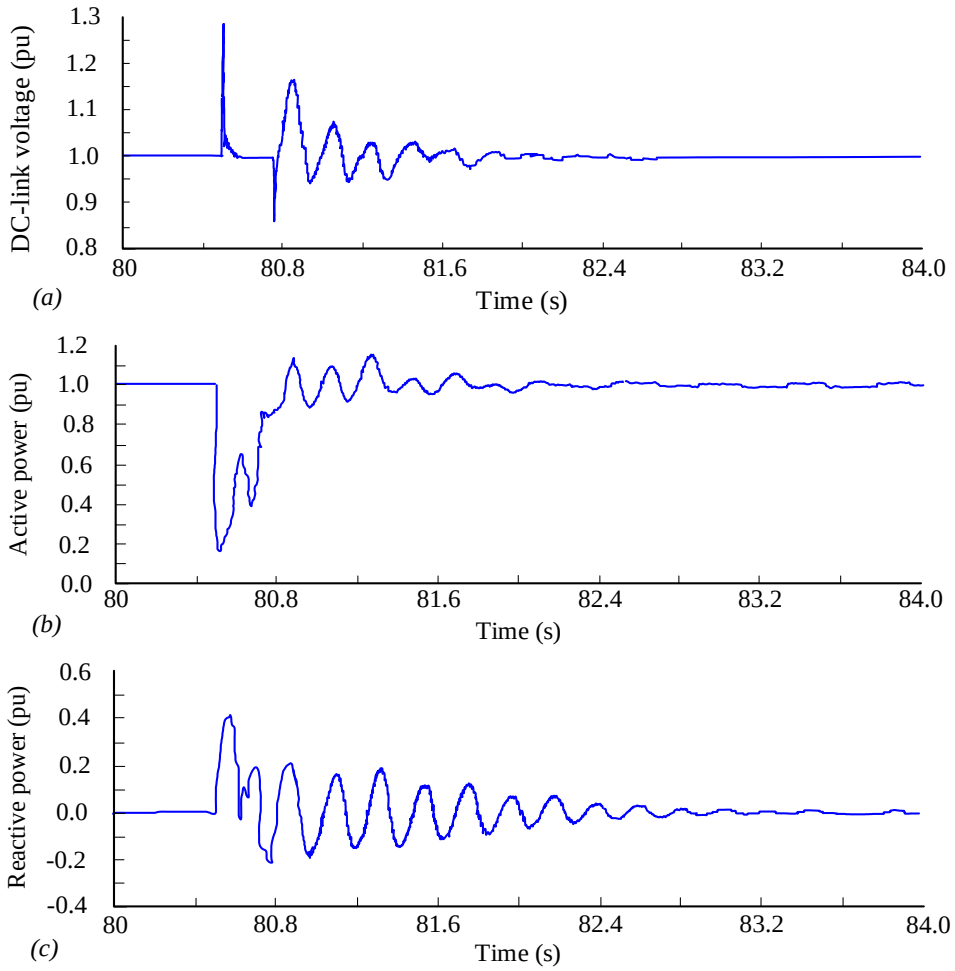

Figure 18. Simulation results of electric variables under fault state: (a) DC-link voltage, (b) active power, (c) reactive power.

5. CONCLUSION

This study describes the power converter configuration system as well as the control strategy for a high-power WECS. The suggested system configuration uses a suitable AC/DC/AC power converter based on DBR with a pulse width modulated current source inverter to drive the PWM-CSI. The generator side converter is developed utilizing the DBR and BBC with the corresponding control strategy for the BBC that allows for maximum power extraction in the proposed configuration. The diode rectifier's output DC current and generator speed are the control variables.

The AC voltage control strategy is given for the PWM-CSI on the grid side to meet two conditions of the integration point between the network and the wind turbine, the voltage at the connection point is equal to 1pu and the frequency of the inverter is contained within the grid frequency. The demand for DC current in PWM-CSI is higher than that provided by DBR to compensate for the extra reactive power required to meet the grid-connected code, resulting in over-voltage on the DC-link when grid faults occur. As a result, a boost DC/DC converter with the appropriate control approach is used to eliminate the over-voltage. In addition, the pitch control approach is used to adjust the wind turbine's output power.

The obtained simulation results summate that the proposed converter configuration and corresponding control strategy for WT-PMSG were very satisfying under the variable wind speed and the three-phase fault conditions. Therefore, this proposed feasibility model can use for further investigation in the wind energy conversion industry. Although the obtained results are interesting and emboldening, some facets may be developed in future works. So, as a viewpoint, we intend to experiment with the proposed system.

Acknowledgement

The author gratefully acknowledge the Industrial University of Ho Chi Minh City for the financial support and the facilities offered during this research.

REFERENCES

[1] Internet Web-Site: re.jrc.ec.europa.eu/pvg_tools/en/tools.html#TMY, M. *GLOBAL WIND REPORT*. 2021, 2021.
[2] Manwell, JF, McGowan, JG, Rogers, AL. Wind energy explained: theory, design and application. Hoboken, New Jersey, US: John Wiley & Sons, 2010.
[3] Jamieson, P, Hassan, G. Innovation in wind turbine design. Hoboken, New Jersey, US: John Wiley & Sons, 2011.
[4] Song, YD, Li, P, Liu, W, Qin, M. An overview of renewable wind energy conversion system modeling and control. *Measurement Control* 2010; *43*(7): 203-208, DOI: 10.1177/002029401004300703.
[5] Alepuz, S, Calle, A, Busquets-Monge, S, Kouro, S, Wu, B. Use of stored energy in PMSG rotor inertia for low-voltage ride-through in back-to-back NPC converter-based wind power systems. *IEEE Transactions on Industrial Electronics* 2012; *60*(5):1787-1796, DOI: 10.1109/TIE.2012.2190954.
[6] Yaramasu, V, Wu, B. Model predictive control of wind energy conversion systems. John Wiley & Sons; 2016.
[7] Giraldo, E, Garces, A. An adaptive control strategy for a wind energy conversion system based on PWM-CSC and PMSG. *IEEE Transactions on power systems* 2013; *29*(3):1446-1453, DOI: 10.1109/TPWRS.2013.2283804.
[8] Cao, W, Xing, N, Wen, Y, Chen, X, Wang, D. New Adaptive Control Strategy for a Wind Turbine Permanent Magnet Synchronous Generator (PMSG). *Inventions* 2021; *6*(1): 3, DOI: 10.3390/inventions6010003.
[9] Golshani, A, Bidgoli, MA, Bathaee, S. Design of optimized sliding mode control to improve the dynamic behavior of PMSG wind turbine with NPC back-to-back converter. *International Review of Electrical Engineering* 2013. *8*: 1170-1180.
[10] Prakash, M, Joo, YH. Fuzzy Event-triggered Control for Back to Back Converter involved PMSG-based Wind Turbine Systems. *IEEE Transactions on Fuzzy Systems* 2021; DOI: 10.1109/TFUZZ.2021.3059949
[11] Yuhendri, M, Ashari, M, Purnomo, MH. Adaptive type-2 fuzzy sliding mode control for grid-connected wind turbine generator using very sparse matrix converter. *International Journal of Renewable Energy Research* 2015; *5*(3): 668-676.
[12] Li, Y, Yuan, X, Li, J, Xiao, H, Xu, Z, Du, Z. Novel grid-forming control of PMSG-based wind turbine for integrating weak AC grid without sacrificing maximum power point tracking. *IET Generation, Transmission Distribution* 2021; *15*(10): 1613-1625, DOI: 10.1049/gtd2.12121.
[13] Sharifian, MB, Mohamadrez, Y, Hosseinpou, M, Torabzade, S. Maximum power control of variable speed wind turbine connected to permanent magnet synchronous generator using chopper equipped with superconductive inductor. *Journal of Applied Sciences* 2009; *9*(4): 777-782, DOI: 10.3923/jas.2009.777.782.
[14] Wang, J, Dai, J, Wu, B, Xu, D, Zargari, NR. Megawatt wind energy conversion system with diode rectifier and multilevel current source inverter. In: *2011 IEEE Energy Conversion Congress and Exposition*; 17-22 Sept. 2011: IEEE, Phoenix, AZ, USA, pp. 871-876, DOI: 10.1109/ECCE.2011.6063862.
[15] Rahimi M. Modeling, control and stability analysis of grid connected PMSG based wind turbine assisted with diode rectifier and boost converter. *International Journal of Electrical Power & Energy Systems* 2017; *93*: 84-96. DOl: 10.1016/j.ijepes.2017.05.019
[16] Wang *J*, Xu D, Wu B, Luo Z. A low-cost rectifier topology for variable-speed high-power PMSG wind turbines. *IEEE transactions on power electronics* 2011; *26*(8): 2192-2200. DOI: 10.1109/TPEL.2011.2106143

[17] Le, V, Li, X, Li, Y, Dong, TLT, Le, C. An innovative control strategy to improve the fault ride-through capability of DFIGs based on wind energy conversion systems. *Energies* 2016; *9*(2): 69, DOI: 10.3390/en9020069.
[18] Dai, L, Tung, D. Modeling for Development of Simulation Tool: A Case Study of Grid-Connected Doubly Fed Induction Generator Based on Wind Energy Conversion System. *International Journal of Applied Engineering Research* 2017; *12*(11):2981-2996.
[19] Nasiri, M, Milimonfared, J, Fathi, SH. A review of low-voltage ride-through enhancement methods for permanent magnet synchronous generator based wind turbines. *Renewable and Sustainable Energy Reviews* 2015;*47*:399-415. DOI: 10.1016/j.rser.2015.03.079.
[20] Wu, B, Lang, Y, Zargari, N, Kouro, S. Power conversion and control of wind energy systems. Hoboken, New Jersey, US: John Wiley & Sons, 2011.
[21] Geng, H, Xu, D, Wu, B, Yang, G. Active damping for PMSG-based WECS with DC-link current estimation. *IEEE Transactions on Industrial Electronics* 2010; *58*(4): 1110-1119. DOI: 10.1109/TIE.2010.2040568.
[22] Wu, B, Lang, Y, Zargari, N, Kouro, S. Power conversion and control of wind energy systems. John Wiley & Sons; 2011
[23] Dao, ND, Lee, DC, Lee, S. A simple and reobust sensorless control based on stator current vector for PMSG wind power systems. *IEE Access* 2018; *7*: 8070-8080, DOI:10.1109/ACCESS.2018.2889080
[24] Wang, CN, Lin, WC, Le, XK. Modelling of a PMSG wind turbine with autonomous control. *Mathematical Problems in Engineering* 2014; *2014***:** 856173, DOI: 10.1155/2014/856173.
[25] Undeland, MN, Robbins, WP, Mohan, N. Power electronics, in Converters, Applications, and Design. Hoboken, New Jersey, US: John Wiley & Sons, 1995.
[26] Mahmoud MM, Aly MM, Abdel-Rahim AM. Enhancing the dynamic performance of a wind-driven PMSG implementing different optimization techniques. *SN Applied Sciences* 2020; *2*(4):1-9. DOI: 10.1007/s42452-020-2439-3.
[27] Evais, A. The effect of wind turbines on subsynchronous resonance. PhD, School of Engineering Cardiff University, Cardiff, UK, 2014.
[28] Etxegarai, A, Eguia, P, Torres, E, Iturregi, A, Valverde, V. Review of grid connection requirements for generation assets in weak power grids. *Renewable Sustainable Energy Reviews* 2015: *41*: 1501-1514, DOI: 10.1016/j.rser.2014.09.030.